

## MECHANICAL DESIGN CONSIDERATIONS FOR BETA=1 CAVITIES

O. Capatina, S. Atieh, I. Aviles Santillana, G. Arnau Izquierdo, S. Calatroni, A. D'Elia, R. Garoby, T. Junginger, D. Maciocha, E. Montesinos, V. Parma, T. Renaglia, T. Tardy, N. Valverde Alonso, W. Weingarten, CERN, Geneva, Switzerland  
S. Chel, G. Devanz, J. Plouin, CEA Saclay, France

### Abstract

The Superconducting Proton Linac (SPL) is an R&D effort coordinated by CERN in partnership with other international laboratories, aimed at developing key technologies for the construction of a multi-megawatt proton linac based on state-of-the-art RF superconducting technology, which would serve as a driver for new physics facilities such as neutrinos and Radioactive Ion Beam (RIB).

Amongst the main objectives of this R&D effort, is the development of 704 MHz bulk niobium beta=1 elliptical cavities, operating at 2 K with a maximum accelerating field of 25 MV/m, and the testing of a string of cavities integrated in a machine-type cryomodule.

The R&D program concerning the elliptical beta=1 cavities fabricated from niobium sheets explores new mechanical design and new fabrication methods. The paper presents several opportunities for design optimization that were identified.

A comparison between stainless steel helium vessel and titanium helium vessel including Nb to Ti transitions is addressed. Different mechanical design aspects, including

cryogenic considerations, and fabrication aspects were analyzed and the results are discussed.

### INTRODUCTION

A first proposal for building a superconducting proton linac (SPL) at CERN to replace some of the existing accelerators was reported about 14 years ago [1], with the potential for evolving towards very high beam power, which would support new physics facilities for neutrinos and/or radioactive ion beams [2]. Later, the design of the SPL evolved towards a low-power 4 GeV version (LP-SPL), with potential use as a new injector chain for the LHC, with the Linac4, presently under construction, as a low energy front-end linac, and having the potential to be up-graded to a multi-MW proton injector [3]. Following recent changes in the mid-term plan strategy at CERN, the construction of the LP-SPL has been stopped, but the continuation of the R&D effort towards a high-power version of the SPL has been endorsed. As one of the priorities of this program, 704 MHz bulk niobium  $\beta=0.65$  and  $\beta=1$  elliptical cavities are to be developed and tested at IPN Orsay [4], CEA Saclay and CERN.

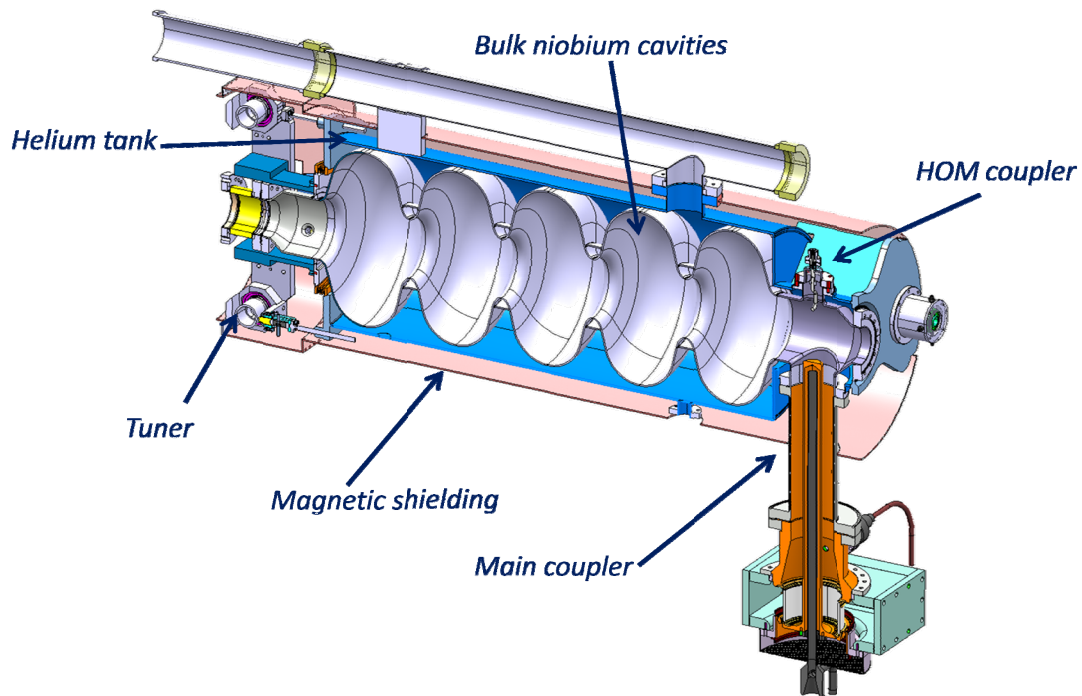


Figure 1: SPL  $\beta=1$  cavity with helium tank, tuner, main coupler, HOM coupler to be tested at CERN in cryo-module.

In an initial phase, at CERN, four  $\beta=1$  cavities will be supplied, and will need to be tested together as they would operate in a machine-type cryo-module [5]. Figure 1 presents the cavity together with its helium tank, the main coupler [6], the HOM coupler, the tuner and the cold magnetic shielding, in the configuration that will be tested at CERN in the cryo-module.

### CAVITY

The main design properties of the  $\beta=1$  cavities are summarised in Table 1, for a 50 Hz pulsed operation, 20 mA current and 0.8 ms beam pulse length.

Table 1:  $\beta=1$  cavity, main design properties & operation.

Property	units	Value
Cavity material	-	bulk niobium
Gradient	MV/m	25
Quality factor $Q_0$	-	$5 \cdot 10^9$
R/Q	-	570
Operating Temp.	K	2
Cryo duty cycle	%	8.22
Dynamic heat load	W	20.4

### RF Design

The RF design of the  $\beta=1$  cavity (Figure 2) has been done at CEA-Saclay [7]. The cavity is asymmetrical: the drift tube at the right of the figure has a diameter of 140 mm, necessary to receive the fundamental power coupler which has a 100 mm diameter. The second drift tube will host the tuning system (Saclay 4 type) and 130 mm diameter is enough. The diameter is reduced at both sides to 80 mm for the connection between two adjacent cavities, provided by flanges.

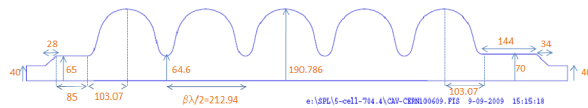


Figure 2: Geometrical parameters of the cavity.

### Mechanical Design

The mechanical design of the cavities ensures their safe use under maximum loading condition during its entire lifecycle.

Since these cavities are aimed to work in the pulsed mode, the sensitivity to the Lorentz force is also especially critical. The effects of the detuning due to those forces were limited by adding stiffening rings in-between the inner cavity half-cells. Figure 3, Figure 4 and Figure 5 present a qualitative comparison between the mechanical deformation of the cavity with and without stiffening rings, under the effect of the Lorentz forces induced by the electromagnetic field.

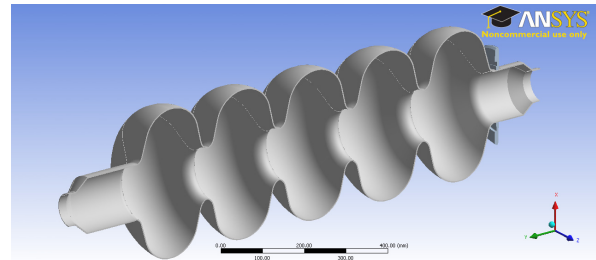


Figure 3: Un-deformed cavity without stiffening rings.

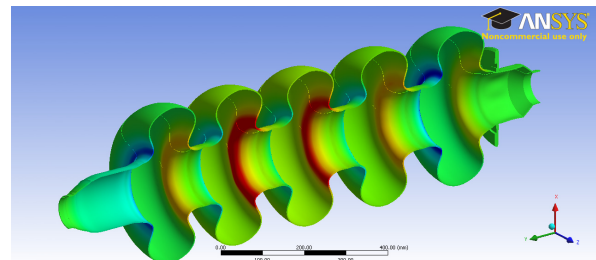


Figure 4: Cavity without stiffening rings deformed due to Lorentz forces.

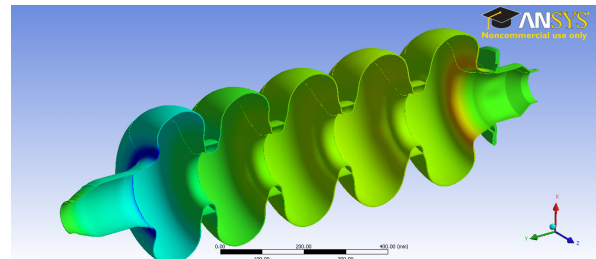


Figure 5: Cavity with stiffening rings deformed due to Lorentz forces.

A final thickness of 3 mm was calculated to be acceptable in order to cope with all the mechanical constraints as well as minimizing the costs of the cavity production.

The manufacturing process induces however a difference in thickness at several locations of the cavity. As an example, spinning process will result in a difference in thickness up to 0.6 mm between the middle of a half cell and the iris or the equator, which represents in our case 20% of the total thickness. The sensitivity of the mechanical behaviour of the cavity to these thickness variations can be quite important.

The mechanical calculations were performed for a cavity presenting non uniform thickness, representative of the manufacturing tests results. The deformation and maximum induced stress were calculated for all load cases during the lifecycle of the cavity, in particular the maximum service pressure (1.5 bars at room temperature and 2 bars at 2 K). The sensitivity to pressure fluctuation has also been checked. The induced detuning is one order of magnitude lower than the RF frequency bandwidth.

The stress induced by tuning the cavity was checked as well as all handling configurations.

Modal analysis (Figure 6) showed the first longitudinal natural frequency at 140 Hz.

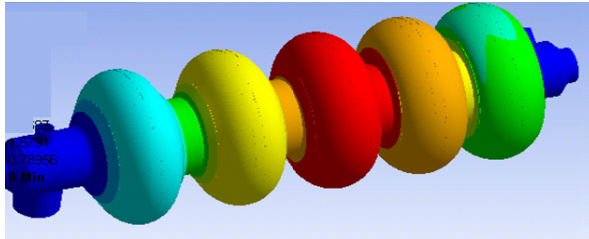


Figure 6: First longitudinal natural frequency at 140 Hz.

The niobium thickness was also checked to be sufficient to withstand buckling against maximum external pressure applied to the cavity.

*Material*

Cavities will be manufactured using high purity niobium. CERN has placed an order to purchase 570 kg of pure niobium. The material in the form of sheets and tubes is intended for the production of four superconducting cavities.



Figure 7: High purity niobium sheets and tubes.

All the material supply follows an extensive series of tests:

- Ultrasonic inspection, for continuity faults and for variations of attenuation (specification attenuation smaller than 20%).
- Surface roughness,  $R_t$  (specification  $R_t \leq 15 \mu\text{m}$ ).
- Hardness, HV10 (specification max. 60 HV10).
- Microstructure, for grain size and uniformity.

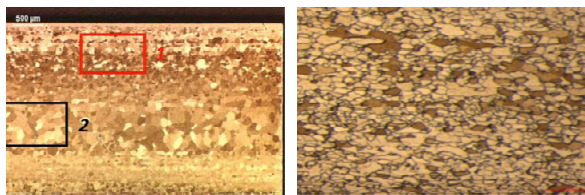


Figure 8: Micrograph of niobium.

- Electrical residual resistivity ratio RRR, in bulk material (specification  $RRR > 300$ ).
- Tensile properties, longitudinal and transverse to rolling direction (specification tensile strengths

min. 140 MPa, yield strengths min. 50 MPa and max. 100 MPa, elongation at break > 40%).

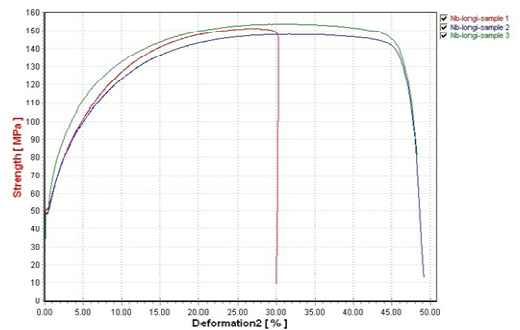


Figure 9: Tensile tests on niobium samples.

*Manufacturing*

A copper cavity mock-up is under fabrication at CERN. It has exactly the same geometry as the future niobium cavities. This mock-up, aimed to be used for real-scale HOM measurements, is also used to set all the manufacturing parameters and to identify possible difficult steps. The processes of fabrication such as mechanical design, shaping and welding of half-cells were done by CERN.

To produce accurate shape, spinning has been chosen as shaping technique (Figure 10) for the half-cells as well as the end groups (Figure 11).

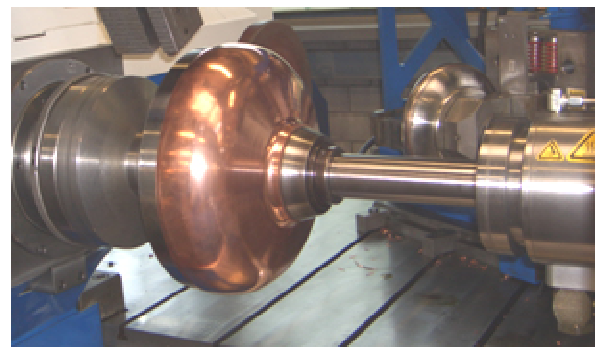


Figure 10: Spinning of Cu half-cell.



Figure 11: Spun end-groups.

The spun half-cells were then machined by turning to improve shape accuracy.

The deviations of the achieved shape with respect to the design profiles were controlled using a coordinate measuring machine (CMM) for all half-cell produced. 22 half-cells were produced and controlled, the achieved shape accuracies are summarized in Table 2 and shape deviations are shown in Figure 12.

Table 2: Shape accuracy of copper spun half cells

	Shape accuracy (μm)
Average shape accuracy	± 150
Shape accuracy min. deviation	± 120
Shape accuracy max. deviation	± 250

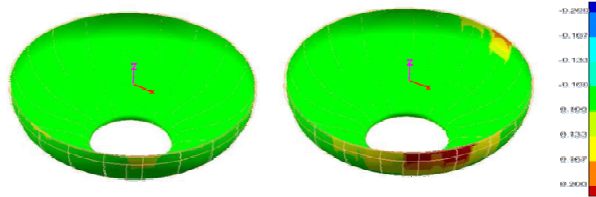


Figure 12: Measured shape accuracy of copper half-cells.

Every process of shaping, surface preparation, assembly and thermal cycling induce a deviation of the final equipment with respect to the ideal geometry. Each process must have its own acceptable deviations. However it is difficult to decide, in an early stage, what is the optimum distribution of the acceptable deviations in-between all these processes. Careful characterization of each operation is then the key of a good understanding of the contribution of each fabrication step to the final RF performance.

Deviation of cell profile from ideal geometry, after each manufacturing steps, is checked by RF measurements for all individual parts and intermediate assemblies.



Figure 13: RF measurement of a copper half-cell.

### R&D for Cold Spray

Achieving high acceleration gradients is the aim of any SRF accelerating cavity fabrication. In order to reduce imperfections on the finished surfaces and contamination on the iris and equator areas, different fabrication procedures have been developed during the past years. The traditional fabrication techniques are based on deep drawing or spinning and electron beam welding (EBW). More recently, some cells have been fabricated using hydroforming technique which permit to obtain seamless cavities and eliminates the risk of weld contamination typical of traditional techniques.

Several attempts have been done to obtain multicell cavities of Nb - Cu material by means of explosive bonding, hot bonding and thermal spray. Nb - Cu clad material instead of bulk Nb is more cost effective, gives thermal stabilization and stiffening rings can be avoided. Nevertheless, clad material has several drawbacks which could be solved by employing a technique called cold spray.

This technique was developed in the 80's and at the present is a relatively common use. Cold gas dynamic spray (cold spray) is based on a supersonic gas (N<sub>2</sub>) jet that propel fine coating powder particles ( +15 μm - 38μm) at very high velocities (500-1200 m/s) resulting on coating formation. The particles are only slightly heated before the impact and the reaction during impact is in solid state. This allows maintaining original chemistry and phases, and only cold working is applied to the materials. The basic principle of cold spray is “adiabatic shear instability”, which also happens in explosive welding.

The main advantages of this technique are that the powders are not melted and there is almost no oxidation during the process. Thin foils and small bending radius (up to 3 mm) can be coated.

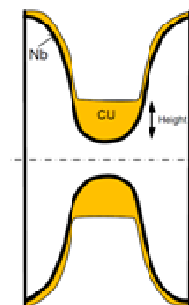


Figure 14: Schematic view of cold-sprayed cavities avoiding stiffening rings.

Moreover, as shown in Figure 14, the cavities could be stiffened against the Lorentz force detuning with the copper layer and an additional copper overlay at the iris [8], [9].

To evaluate the convenience of this technique for fabrication of seamless multi-cells cavities two niobium sheets (120 mm x 120 mm x 1mm) have been cold

sprayed with copper, tests will be performed to assess coating and bonding strength and the effect of thermal cycling. The preliminary test plan is detailed in Table 3:

Table 3: Test on cold sprayed samples.

	W/O HT	W/ HT (800°C/2h)	Status
Thermal shock (10 x in liquid N <sub>2</sub> )	no	yes	Ongoing
Microstructure observation	yes	yes	Ongoing
Thermal conductivity	yes	yes	Ongoing
Bending test	yes	yes	Ongoing
Shear test	yes	yes	Ongoing
Tensile test	yes	yes	Ongoing

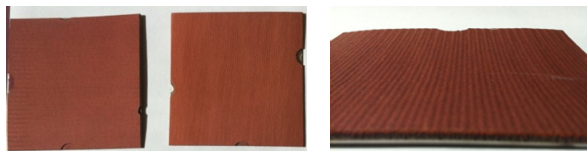


Figure 15: Two samples of Cold spray (Nb 1mm + sprayed -Cu 2mm).

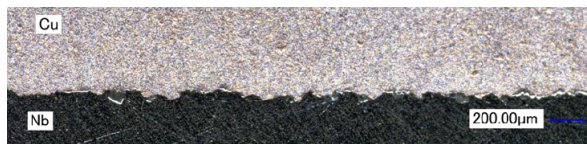


Figure 16: Macrograph of cold-sprayed copper on niobium.

During the next step, a tubular coating tensile test (TCT-test) [10] will be performed to provide information regarding mechanical coating strength, deposition efficiency and coating microstructure.

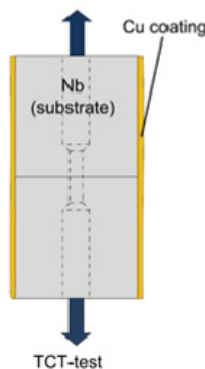


Figure 17: TCT-test configuration.

The combination of seamless cavities and Nb - Cu cold sprayed material could become an alternative to the actual

manufacturing techniques. Hydroforming followed by cold spray could become a very good solution for SRF cavities manufacturing since the welds would be avoided as well as the stiffening rings, and the cavities could be easily hydroformed because of the small thickness of the niobium plate (~ 1 mm Nb + 2 mm sprayed copper).

## HELIUM TANK

### Tank Dimensions for Heat Load Extraction

The helium tank will contain saturated superfluid helium at 2 K cooling the cavity and allowing the extraction of the heat dissipated into the bulk niobium wall by the RF electromagnetic field, as well as the heat injected by all the adjacent components such the main power coupler. The geometry of the helium tank has thus to allow this heat extraction while optimising the quantity of the helium to be used.

The operating point of the SPL cavities with respect to the helium phase diagram is shown in Figure 18.

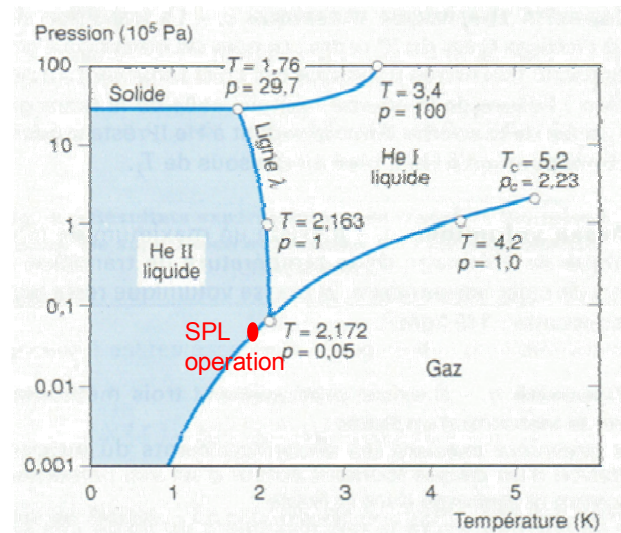


Figure 18: Helium phase diagram and SPL operating point.

The cavity is cooled by saturated superfluid helium. However, the cavity wall from which the heat has to be extracted is at a certain depth below the liquid-vapour interface. Thus, without any heat being applied, the state of the helium can be described by the red dot in Figure 19. The pressure applied at the heat transfer surface is therefore  $p = p_0 + \rho gh$ . If heat is applied to induce heat transfer in the system, there will be a local temperature excursion  $\Delta T$ . The “stab margin” in Figure 19 represents the maximum value of this temperature excursion before meeting the liquid-vapour interface at which point boiling begins [11]. As an example, in saturated He II at 2 K, a channel of  $L=10$  cm height results in a hydrostatic over-pressure of  $\Delta p = 1.4$  mbar, creating a temperature margin up to point boiling from 2 K to ~2.025 K.

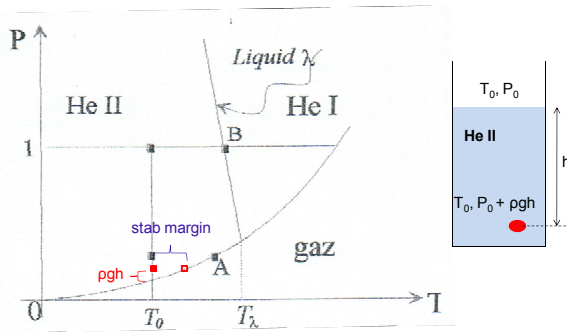


Figure 19: Stabilization margin for saturated He II due to hydrostatic pressure.

Superfluid helium is an excellent thermal conductor. A typical value of “thermal conductivity” at 2 K is 2 kW/mK for a channel of cross section of 1 cm<sup>2</sup> and length 10 cm, which represents one order of magnitude higher than pure copper. However, this relationship is true only for small heat fluxes. Above a critical heat flux, the temperature increases drastically and eventually the superfluidity is lost. The heat flux in He II depends on the temperature and on the channel dimension.

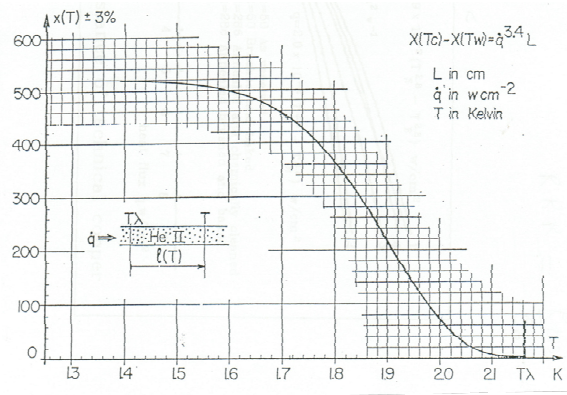


Figure 20: Claudet et al. – Experimental values of heat transfer by He II.

Gorter and Mellinck have shown the dependence of the heat flux density with respect to the externally applied temperature in superfluid helium. Claudet et al. [12] gave experimental values of heat transfer by He II (Figure 20).

Applying the theory to our geometry, in some positions, the maximum heat load extracted by the superfluid helium is limited to 0.8 W/cm<sup>2</sup>. For the port to be connected to the bi-phase tube, this maximum heat load extracted is 1.5 W/cm<sup>2</sup>. The dynamic heat load to be extracted in pulsed operation is 20 W. To this value the static heat load from the cryo-module and the main coupler have to be added. If the cavity needs to be tested in CW mode, then the helium tank port will be of minimum 167 cm<sup>2</sup> since ~250 W should be extracted.

*Minimizing the Injected Heat Load*

The heat dissipated by the fundamental power coupler at the interface to the helium tank has also been estimated

and an actively cooled Double walled Tube was optimised in order to minimize these losses.

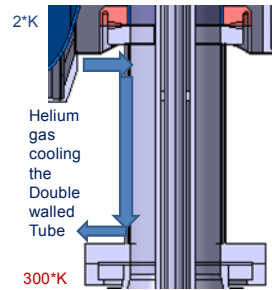


Figure 21: Main coupler actively cooled Double walled Tube at the interface to the helium tank.

The heat injected to the helium tank by the main power coupler was estimated to more than 20 W if no active cooling of the Double walled Tube. When actively cooling the main coupler Double walled Tube using helium gas at 4.5 K, the heat loss to helium tank is reduced to negligible values (Figure 22).

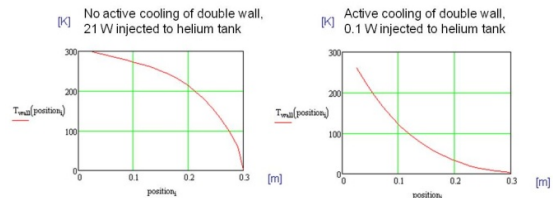


Figure 22: Temperature profile in main coupler Double walled Tube without and with active cooling.

*Mechanical Considerations*

The helium tank has also a structural role since it transmits the effort applied by the tuner to the cavity, its rigidity being thus very important in the tuning process. The stiffness of the helium tank has a direct impact on the Lorentz detuning, defining the boundary conditions of the cavity. A longitudinal stiffness higher than 100 kN/mm is required.

Two choices of material have been studied for the helium tank: stainless steel and titanium. The titanium has the advantage of the same thermal contraction as niobium (in the order of 1.5 mm/m from ambient temperature to 2 K), while the thermal contraction of the stainless steel is approximately the double. The use of stainless steel tank would induce either the need of a larger tuner range than in the case of titanium tank or larger thermal stresses to the cavity.

The advantage of the stainless steel is the manufacturability and thus the cost.

One of the driving elements for the mechanical design was the transitions from the helium tank to all the adjacent components, in particular the main coupler. This analysis is detailed in the chapter below. The baseline for the β=1 cavities that will be tested in a cryo-module at CERN is stainless steel helium tank.

### Niobium to Titanium Transitions

Both titanium and stainless steel helium tanks have been designed and their feasibility checked.

An alloyed version of titanium was preferred to pure titanium, even if the pure one is more “classically” used in other Institutes as material of helium tanks hosting RF cavities. The grade 5 titanium Ti6Al4V is significantly stronger than the commercially pure titanium while having the same stiffness and thermal properties. This grade is heat treatable, already used in many cryogenic applications and is an excellent combination of strength, corrosion resistance, weldability and fabricability.

Its mechanical properties allow also its use for manufacturing of ConFlat (CF) flanges, cheaper than the NbTi flanges usually utilized when titanium helium tanks are chosen.

One possible solution for the interfaces of the accelerating cavity to the helium tank is a welding between Nb and Ti6Al4V. The great differences in physical characteristics, call for particular considerations on the welding process. The sensitivity to the presence of oxygen and hydrogen which reduce notably the ductility of the base materials makes the electron beam welding under high vacuum conditions a suitable process to achieve a high quality welds.

Electron beam process was used for welding high purity ( $RRR \geq 300$ ) Niobium to a Titanium alloy (Ti6Al4V). Analysis of the welding before and after degassing heat treatment ( $800^\circ\text{C}/2\text{h}$ ) was based on NDT (dye penetrant and X-Rays), mechanical tests before and after heat treatment (tensile tests and microhardness profiles), macro and microstructural assessment via optical and scanning electron microscopy. The cross section of weld macrostructure is shown in Figure 23.

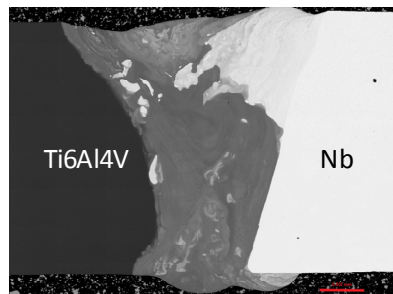


Figure 23: Macrograph of electron beam weld of niobium to Ti6Al4V.

The average tensile strength before heat treatment (HT) was  $152.7 \pm 2.7$  MPa with an average elongation at break of  $24.8 \pm 2.7$  %. After HT, the average tensile strength was  $158.8 \pm 2.2$  MPa with an average elongation at break of  $26.6 \pm 0.1$  %. All samples broke in the bulk Niobium.

HV0.05 hardness measurements were performed. The hardness of the weld metal zone is ranging from 201 to 311 HV0.05, what is an intermediate value between the hardness of both parent metals. Samples after HT did not show substantial differences in the hardness values compared to the samples before HT (Figure 24).

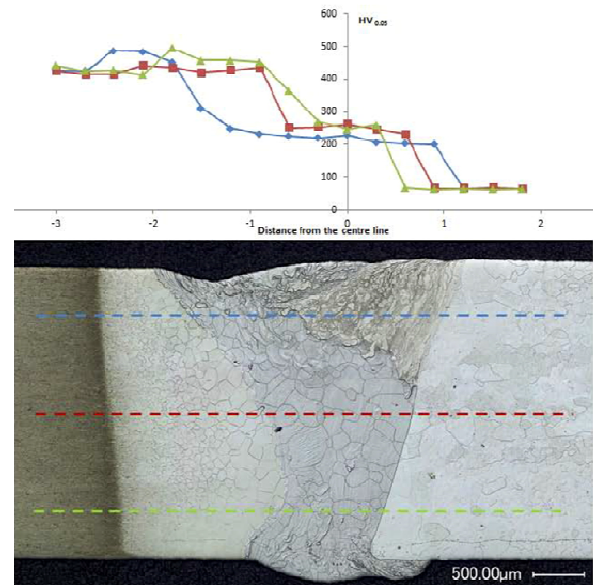


Figure 24: Hardness profile across the weld.

EDS semi-quantitative analyses were performed in order to assess the composition of the weld bead. For the samples after HT, there is no remarkable difference in terms of composition.

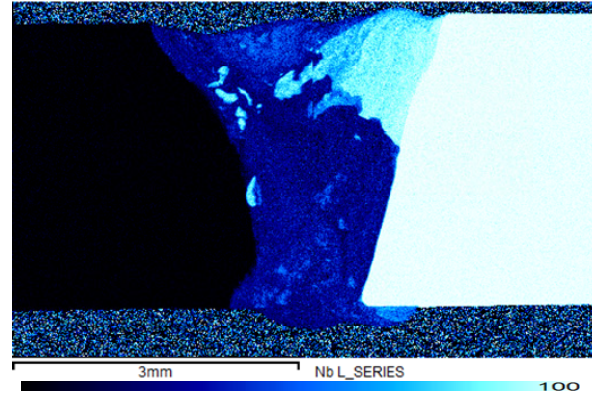


Figure 25: EDS quantitative map representing the weight percentage of Nb.

Results showed no weld defect or mechanical weakness. As a first conclusion, this transition from Grade 5 titanium to pure niobium, by electron beam welding, could be safely used for our application.

### Titanium to Stainless Steel Transitions

The components adjacent to the helium tank are usually made of stainless steel. In particular, the main coupler double wall to be connected to the helium tank is manufactured in 316LN stainless steel. If titanium helium tank is used, then transitions from titanium to stainless steel have to be carried out. CF flanges connection could be one option and was investigated. The titanium thermal contraction from 300 K to 2 K is the half of the thermal

contraction for stainless steel and copper. Thus, the difference in thermal contraction could generate leaks at cryogenic temperatures. This becomes even more critical with increasing dimensions. The solution was checked for the biggest diameter: DN 100 simulating the case of the main coupler flange.

A set-up was created to reproduce the transition from a helium tank titanium CF flange and the main coupler stainless steel CF flange, used with a “LHC type” RF gasket. The assembly has been tested several times at liquid nitrogen temperature. Leak-tightness was lost after several thermal cycles for gaskets that had dimensions slightly out of specifications. The gaskets manufactured within specification were successfully cycled up to 5 times with leak-tightness better than  $1 \cdot 10^{-10}$  mbar\*s.

We can conclude that this solution could be a valid one; however its reliability depends very much on manufacturing parameters and has to be extensively checked.



Figure 26: Ti6Al4V and 316LN CF flanges with OFE copper RF gasket tested at liquid nitrogen temperature.

### Niobium to Stainless Steel Transitions

The stainless steel solution for the helium tank has also been investigated and represents the baseline solution for the  $\beta=1$  cavities that will be tested in a cryo-module at CERN. The transition to the adjacent components in stainless steel is straightforward since stainless steel to stainless steel ConFlat flanges are extensively used at cryogenic temperature.

Fusion welding of niobium and stainless steel was difficult to implement because it generates brittle phases (intermetallic compound) in weld. It showed that the basic reason of the embrittlement of the joint was the emergence of continuously distributed intermetallics. On top of that, physical and mechanical properties present big differences in thermal conductivity and linear expansion coefficient between the two base metals, which would lead to large temperature gradient and thermal stress in the joint during the welding. Less literature about successful fusion welding of these two alloys has been reported. On the other hand, brazing can eliminate the problems in fusion welding because the base metals remain in the solid state during joining. Furthermore, this brazing technique has been developed at CERN and many successful examples were reported [13], [14].

In addition to the well mastered niobium to stainless steel brazing technique, a R&D program has started at

CERN aiming to explore electron beam welding possibilities between niobium and stainless steel.

Based on the advantages of high energy density, precisely controllable heating position and radius, electron beam welding was the most frequently utilized fusion welding technique in the field of joining of dissimilar metals. A pure copper (OFE Cu) interlayer sheet was adopted in the present work to join niobium and 304 L stainless steel by electron beam welding.



Figure 27: Schematic view of weld configuration using a copper interlayer.

The first pass acted on the copper layer near the interface between niobium and copper, the second pass acted on the interface between copper and stainless steel with identical beam parameters for both of them. Figure 28 shows the surface features of the Nb/304L joints electron beam welded with the transition via a pure copper insert sheet in contact face.



Figure 28: Surface features of Nb/304L joints electron beam welded with copper transition.

Microstructure observation and composition measurement are undergoing. In the preliminary tests according to this configuration, the macrograph of the weld is characterized by full penetration. Furthermore, it could also be seen that there was solid solution of copper uniformly distributed in weld, which improves the plasticity of the joint. Absence of intermetallics that might fragilise the weld is still to be carefully checked.



Figure 29: Macrostructure of cross section of weld.

The joint was achieved by typical fusion welding process. The first promising results have however still to be complemented with detailed microstructure analysis of the joint, phase constitution and mechanical properties at room temperature, high temperatures as well as at cryogenic temperatures.

### MAGNETIC SHIELDING

To achieve Q-values above  $10^9$  the earth magnetic field needs to be reduced on the cavity surface. For the SPL a requirement of less than  $1 \mu\text{T}$  residual DC magnetic field was defined. This corresponds for high RRR niobium at 704 MHz to a residual resistance of less than 3 nOhm [15]. Electromagnetic simulations using CST EM studio showed that the earth magnetic field can best be shielded by a combination of inner and outer cylinders as presented in Figure 30.

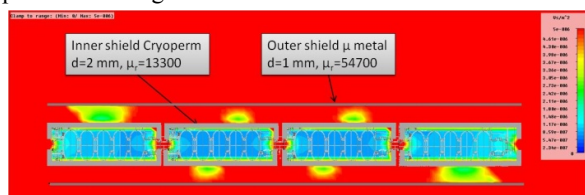


Figure 30: Magnetic shielding for a string of 4 cavities.

If one uses only one shield the shielding factor is proportional to the thickness of the material and its permeability. For two shields not too close to each other the achieved shielding factor is the product of the two shielding factors. The inner cylinders should be as close as possible to the cavity. One shield per five-cell cavity is necessary to avoid demagnetization. These cylinders must be equipped with end-caps to meet the requirement of less than  $1 \mu\text{T}$  residual field over the whole cavity surface. The outer cylinder should not be too close to the inner cylinders. The solution found is one cylinder per module (4 cavities). End-caps are not necessary here. Results on test cylinders manufactured for TESLA cavities showed that  $\mu_r$  values of 54700 (Mu-metal at room temperature) and 13300 (Cryoperm at 4K) can be achieved [16]. From these values it was found that the requirement of less than  $1 \mu\text{T}$  residual field can be met by 2 mm thick inner cylinders made of Cryoperm and 1 mm thick outer cylinders made of Mu-metal [17].

### SUMMARY AND OUTLOOK

A string of four SPL superconducting  $\beta=1$  RF cavities will be installed by 2013 in a so-called Short cryo-module and will be tested at CERN in a machine-type configuration, powered by high-power RF.

Extensive studies have already been done with respect to the mechanical aspects of the cavities and helium tank, and the construction of these four cavities is foreseen by the end of 2012.

In the frame of the SPL R&D study, innovative mechanical solutions have already been explored and a number of R&D studies are still ongoing with several promising results already obtained.

### REFERENCES

- [1] R. Garoby and M. Vretenar, CERN/PS/RF/Note 96–27.
- [2] M. Vretenar, CERN Report No. CERN-2000-012, <http://doc.cern.ch/yellowrep/2000/2000-012/p1.pdf>.
- [3] O. Brunner et al. “Assessment of the basic parameters of the CERN Superconducting Proton Linac”, Physical Review Special Topics-Accelerators and Beams, 12, 070402 (2009).
- [4] G. Orly et al. “SPL Cavity Development”, SRF2011, Chicago, July 2011.
- [5] V. Parma et al. “Conceptual design of the Superconducting Proton Linac (SPL) short cryo-module”, SRF2011, Chicago, July 2011.
- [6] E. Montesinos, Conceptual SPL RF Main Power Coupler design, sLHC Project Report-0052, 16 March 2011.
- [7] J. Plouin et al. “Optimized RF design of 704 MHz  $\beta=1$  cavity for pulsed proton drivers”, SRF2011, Chicago, July 2011.
- [8] S. Bousson, “Advances in superconducting RF cavity stiffening by thermal spraying”, for the IPN/LAL/CEA collaboration. Institut de Physique Nucleaire (CNRS-IN2P3), Orsay, France.
- [9] T. Schmidt, F. Gartner, H. Assadi, H. Kreye, “Development of a generalized parameter window for cold spray deposition”, Acta materialia 54 (2006) 729-742.
- [10] T. Schmidt, F. Gartner, H. Kreye, “Tubular coating tensile test”, Helmut Schmidt University, March 2008.
- [11] S. Van Sciver “Helium Cryogenics”, Plenum Press, New York.
- [12] G. Bon Mardion, G. Claudet, P. Seyfert, “Practical data on steady state heat transport in superfluid helium at atmospheric pressure”, DTCE/SBT CEA France, 1978.
- [13] J.P. Bacher, E. Chiaveri, and B. Trincat, “Brazing of niobium to stainless steel for UHV applications in superconducting cavities”, CERN/EF/RF 87-7, 1987.
- [14] J.D. Fuerst, W.F. Toter and K.W. Shepard, “Niobium to stainless steel braze transition development”, ANL, Argonne, IL 60439, USA.
- [15] H. Padamsee et al. “RF Superconductivity for Accelerators”, John Wiley & Sons, Inc.
- [16] TESLA-Report 1994-23.
- [17] T. Junginger, “Magnetic shielding simulations for SPL cryo-module”, 5th SPL collaboration meeting, CERN, November 2010.